Generation of highly charged ions of heavy elements in a CO_2 laser plasma

K. N. Makarov, Yu. A. Satov, A. P. Strel'tsov, V. K. Rerikh, and A. E. Stepanov

Troitsk Institute of Innovative and Thermonuclear Research, 142092 Moscow, Russia

O. B. Shamaev and B. Yu. Sharkov

Institute of Theoretical and Experimental Physics, 117257 Moscow, Russia

H. Hazerot, K. Langbein, and T. R. Cherveud

Centre Européene de la Recherche Nucléaire (CERN), PS Division, Geneva, Switzerland
(Submitted 14 June 1994; resubmitted 25 July 1994)
Zh. Eksp. Teor. Fiz. **106**, 1649–1662 (December 1994)

We present experimental and theoretical results of studies of the generation of highly charged Pb and Ta ions in a plasma created by CO_2 laser pulses with power densities of $4\cdot10^{13}$ and $6\cdot10^{14}$ W/cm^2 and pulse durations of 30 and 2.5 ns respectively. We have measured the ion content of the plasma and the energy spectra of the ion component of the current at considerable distances from the target. We found that the total current density created by the Pb^{+25}–Pb^{+32} ion group was 1.5 mA/cm^2 at a distance of 3 meters. We formulate requirements on a laser system intended for use as a source of multicharged ions, and present results of numerical calculations for the problem based on one- and two-dimensional models. The latter allow us to obtain quantitative agreement with experiment.

1. INTRODUCTION

The action of high-power laser radiation on a solid-state target is accompanied by the creation of a high-temperature plasma. By studying the characteristics of the latter in the expansion stage, we can uncover details of the ablation process and the interaction of the radiation with the plasma.

Heavy-element plasmas are of particular interest for many reasons, including practical applications (laser thermonuclear fusion, ion sources, etc.). In order to study the relationship between the ion content of such a plasma and the characteristics of the radiation that creates it, we must conduct experiments over a wide range of laser pulse parameters and develop a computational-theoretical model that describes the laser plasma at different stages of its expansion. This paper presents the first results obtained in the course of a joint effort that included European organizations devoted to laser investigations, the Troitsk Institute of Innovative and Thermonuclear Studies, and the Institute of Theoretical and Experimental Physics.

2. DESCRIPTION OF THE EXPERIMENTAL SETUP

Our first experiments were carried out using the TIR-1 apparatus, which was thoroughly described in Ref. 1. The TIR-1 scheme can be used to generate CO_2 laser pulses with stable parameters and durations that can be varied in the range 2 to 30 ns. Gas-phase saturable absorbers eliminated feedback between the target under study and the laser system. The wave front of the radiation was shaped by spatial filters and matched irises, so that an output beam with diameter 200 mm had a divergence that was close to diffraction-limited. The laser system characteristics ensured good repeatability of the measurement results and optimization of the laser pulse parameters from the start.

In the experiments described below, the laser source was a single-mode CO_2 oscillator built around the preamplifier module of the TIR-1 apparatus, with an active volume of ~17 liters. The radiation was produced in an unstable resonator of length 2.7 m and an amplification of ~3. The energy of the output beam of diameter 150 mm was between 120–130 J (for a CO_2:N_2:He mixture with composition 4:1:5). The time to form the pulse was typical of a CO_2 laser at atmospheric pressure in the regime of phase-locking of the longitudinal modes. The envelope of the signal consisted of a peak with a FWHM duration of 25–30 ns and a relatively long (~1 μs) "tail," containing about half the energy.

Experiments with focusing of the radiation showed that the distribution of radiation in the far field was well described by diffraction of a plane wave by the ring-shaped output aperture of the unstable resonator, whose external and internal diameters were 150 mm and 50 mm respectively. The laser beam concentrated 50% of its energy in a central spot with diameter ~50 μm at a level of $1/e$ ($F=600$ mm), corresponding to a diffraction divergence of $7\cdot10^{-5}$ rad. The rest of the radiation was distributed in "wings" formed by a concentric system of diffraction rings, which fell off in intensity from the center to the periphery.

Temporal and energy measurements were made of the laser pulses for each shot by using an optical scheme in which part of the radiation was removed by a reflecting wedge. The energy of each pulse was recorded with an EP-50-02 calorimeter on a C8-13 oscilloscope. The temporal shape of the radiation was recorded on an ARC TURBO 12 PC using a pyroelectric detector made of the crystal $LiNbO_3$ (time resolution <200 ps) and digitized oscilloscope traces.

The radiation from the laser source was focused by a mirror ($F=600$ mm) normally onto the target surface. A target made of metallic Pb or Ta was placed in a vacuum chamber pumped down to a pressure of ~10^{-6} torr. Mea-

 1063-7761/94/120891-08$10.00

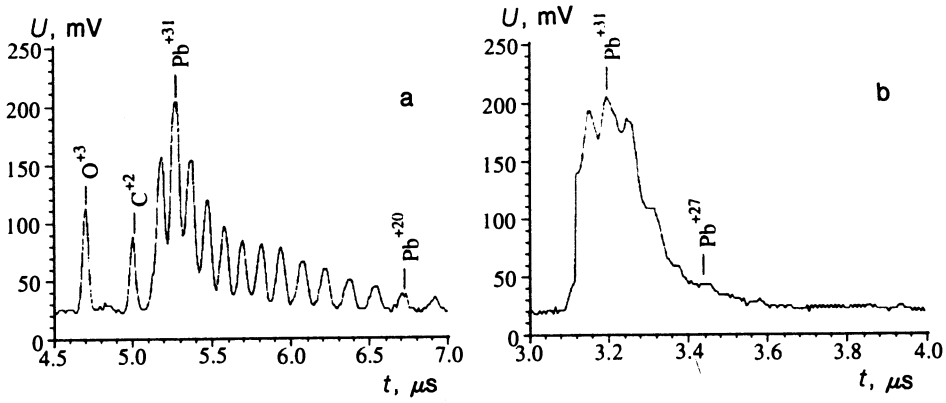

FIG. 1. Typical signals from the electrostatic analyzer for the TIR-1 setup: (a) power density $P_0=4\cdot10^{13}$ W/cm^2, pulse length $\tau=30$ ns; (b) $P_0=6\cdot10^{14}$ W/cm^2, $\tau=2.5$ ns.

surements were made of the characteristics of the ions in the plasma as it passed through the central aperture (diameter 25 mm) of the mirror. The energy spectra of the ionic components were recorded over a wide range of energies and charges; the signal due to the ion current was measured 1.5 and 3 m from the target. To accomplish this, we used an electrostatic analyzer with an angle of rotation of 90° and an ion collector operating in the regime of current recording, both well-described in the literature. The construction and details of the parameters for these instruments are given in Ref. 2. The measured signals were recorded using a digital oscilloscope on a personal computer.

Separate experiments were carried out using a LUMONICS TEA 601 CO_2 laser and a magnetic spectrometer.

3. EXPERIMENTAL RESULTS

Lead ions with charges $z>20$ are generated in the plasma at a power density $\geqslant10^{13}$ W/cm^2 at the target. The ionic composition depends significantly on the space-time characteristics of the radiation. For pulses consisting of a solitary peak with duration 25–30 ns, the ionic component consists of a group of highly charged ions (five to seven successive ionization states); under our conditions this group contained practically no low-charge ions when the position of the focus coincided with the surface of the target to an accuracy of ±100 μm ($F=600$ mm). For larger displacements of the target from the position of exact focus, a considerable number of ions with lower charges appear. This is connected with changes in the distribution of radiation at the target surface, and a concomitant increase in the role of zones with lower intensities. The presence of a low-intensity tail in the radiation pulse also introduces low-charge states. When we shortened the duration of the pulse to 2.5 ns while simultaneously increasing the power density by a factor of 15, there was no appreciable increase in the charge states of the ions (compare typical signals from the electrostatic analyzer in Fig. 1); therefore, we used a single-mode oscillator for the ion source. The following important fact should be noted, which is related to the conditions for the applicability of our oscillator scheme. When the oscillator and target are placed close to one another, oscillation takes place in the resonator formed by the laser mirrors and target surface (later by the plasma boundary) combined with the focusing objective. As a result, the intensity of the radiation pulse decreases, which significantly degrades its spatial characteristics and hence lowers the power density at the target considerably. In order to avoid this undesirable effect we introduced an additional optical path length L such that the round trip time is $t=2L/c>t_1+t_2$, where t_1 is the time for development of the oscillations and t_2 is the duration of the primary radiation peak. This is illustrated by the signals from the analyzer (Fig. 2) obtained for the LUMONICS laser. When an optical decoupler is present (Fig. 2b) the charge states are considerably higher, and a group of high-charged ions is selected out. This method does not guarantee the absence of parasitic oscillations for $t>2L/c$ with a corresponding increase in the fraction of low-charge ions. It is possible to improve things further by introducing a gate (for instance, a plasma gate) that would cut off the oscillator from the target after the principal radiation peak passes through.

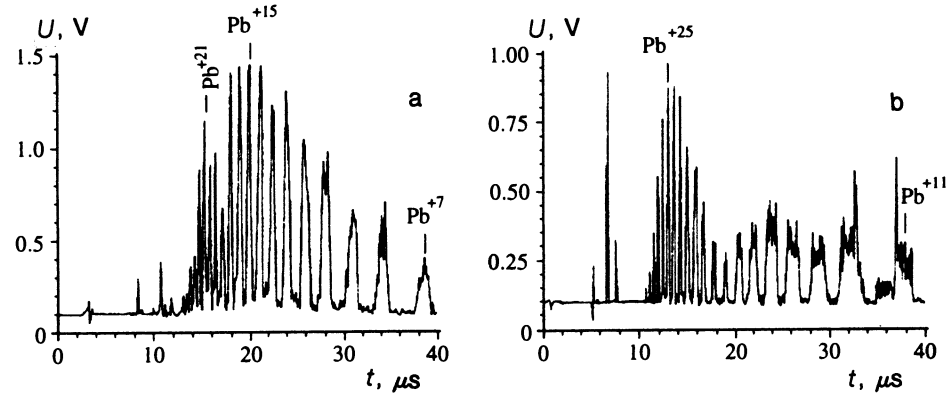

FIG. 2. Signals from the electrostatic analyzer obtained from the LUMONICS setup (CERN): (a) without optical decoupling; (b) after introducing an optical decoupler.

The ion spectra were measured by varying the voltage on the analyzer plates from 50 V to 3.9 kV from shot to shot. The signals in Fig. 3 correspond to the central portion of the energy spectrum of the high-charge-state group of ions. The analyzer signal was processed without taking into account the effect of secondary emission of electrons, assuming that the latter is a weak function of the average ion charge $\langle z \rangle$ for $\langle z \rangle = 30 \pm 4$. The spectra obtained are shown in Figs. 3a and 3b. Noteworthy is a twofold to threefold increase in the ion energy when a high-power nanosecond pulse is used. Fig. 3c is the spectrum of the ion component at a power density of $\sim 10^{12}$ W/cm^2. In this case, the radiation from an oscillator with energy 20 J was focused by a lens with $F = 2000$ mm.

The total ion current collector signals at distances 3 and 1.5 m, which correspond to the spectra shown in Figs. 3a and 3c, are shown in Figs. 4a and 4b respectively. These current signals saturated as a function of the voltage used to extract the ion beam, and were not distorted by secondary electron emission.[2] The values of current density were averaged over the 25 mm aperture and the transmission of the collector grid was taken into account.

The available experimental material allows us to estimate the error connected with ignoring the coefficient of secondary emission. The ion spectrum (Fig. 3c) was summed over the entire recorded range of charges (from 1 to 12) and velocities (from $2.5 \cdot 10^6$ to $2.2 \cdot 10^7$ cm/s). The signal obtained in this way (Fig. 4b, curve *2*), which is normalized by the amplitude of the collector current, can be compared with the real current in the region of low-charged ions. The comparison shows that the secondary emission coefficients for Pb^{+10} ions with energies of about 10 keV and Pb^{+1} ions with energies in the range 1 to 2 keV differ by no more than a factor of 2.5–3. Since the different value of the current in the low-energy interval can be related to ions from the plasma that are unrecorded by the analyzer at the walls of the time-of-flight analyzer or the collector grid, this is an estimate based on the maximum.

4. COMPUTATIONAL MODEL

We calculated how the ion composition arises in a plasma obtained by heating a lead target with radiation from a CO_2 laser using one-dimensional and two-dimensional numerical models of the plasma dynamics combined with equations based on an atomic model of the lead ions. In the case of the one-dimensional model, the calculations were carried out in a spherical geometry. The gas dynamics of the plasma was described in the single-fluid two-temperature approximation. We did not take into account the influence of electric fields that arise as the charges separate and in the system used to extract the ion beam. We did take into account the electron thermal conductivity, the energy exchanged between electron and ion components (temperature relaxation), and also the heat release due to absorption of the laser radiation. We also included a term in the energy balance equation for the electron component that describes the energy expended in ionizing and exciting the ions in the plasma, and, accordingly, the heat released during three-body recombination. We neglected the influence of radiation by the plasma on its gas dynamic and ion content.

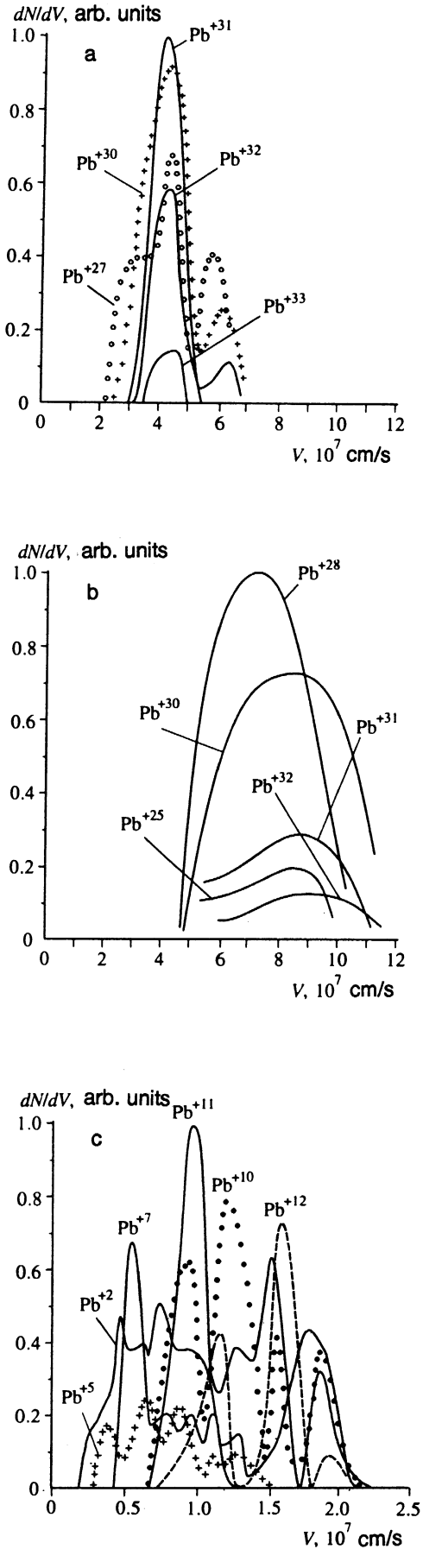

FIG. 3. Spectrum of lead ions versus velocity V: (a) $P_0 = 4 \cdot 10^{13}$ W/cm^2, $\tau = 30$ ns; (b) $P_0 = 6 \cdot 10^{14}$ W/cm^2, $\tau = 2.5$ ns; (c) $P_0 = 10^{12}$ W/cm^2, $\tau = 30$ ns.

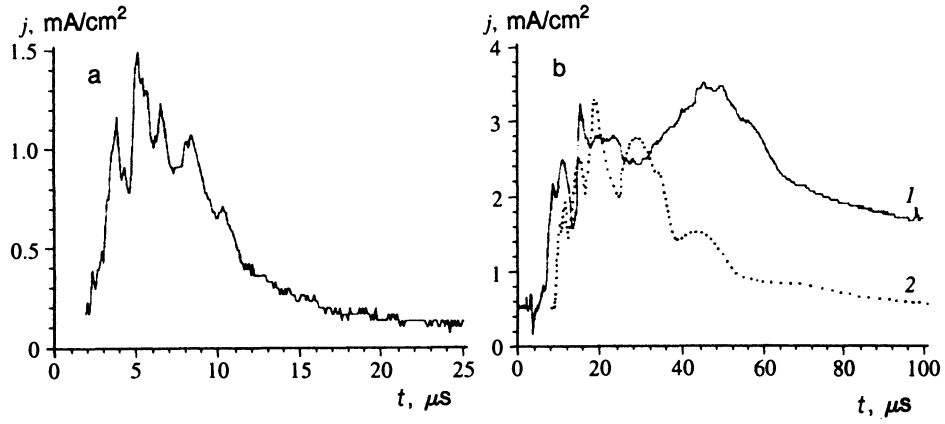

FIG. 4. Collector signals for total ion current: (a) $P_0=4\cdot10^{13}$ W/cm^2, pulse length $\tau=30$ ns; (b) $P_0=10^{12}$ W/cm^2, $\tau=30$ ns (*1*—measured, *2*—reproduced based on the ion spectrum of Fig. 3c).

The boundedness of the electron heat conduction flux was taken into account by limiting it at a level of 0.1 of the convective flux. Absorption of the laser radiation was modeled in the geometric-optics approximation.

In the one-dimensional model we assumed radial illumination from all sides. In the radial direction, which in this approximation is a characteristic of the transport equation, we solved the one-dimensional steady-state transport equation for the laser radiation. In our model the laser radiation was absorbed according to a inverse-bremsstrahlung mechanism down to the critical density; an additional 5% of the power was absorbed on the critical surface while the rest was reflected. In the two-dimensional code the propagation and absorption of the laser radiation were modeled by a more detailed ray-tracing method. The laser beam consisted of a set of rays distributed randomly across the beam at each time step. Each ray was then traced through the computational grid until it passed beyond the bounds of the latter or was completely absorbed. In the approximation of constant electron density gradient in each cell, the trajectory of the ray in a cell is a segment of a parabola. This allowed us to determine the optical thickness of the cell and the fraction of energy absorbed. This type of model is adequate to describe classical bremsstrahlung absorption. Correct simulation of anomalous absorption in the region of the critical surface requires a considerable amount of computation to solve the Maxwell equations on a fine grid and is a problem of interest in its own right. In the two-dimensional model we used an empirical model of anomalous absorption, described in detail in Ref. 3.

5. ATOMIC MODEL

Since we must simulate the kinetics of atomic-level populations for heavy-element ions, it is necessary to have a large amount of atomic data. Compiling this data for multielectron systems is extremely time-consuming. Therefore, when we need information on the ion content of the plasma (that is, the total numbers of ions of each charge state) it is desirable to have a simpler kinetic model which allows us to obtain the required atomic data set rather quickly for a wide range of chemical elements, and, at the same time, allows us to describe correctly the dynamics of the ionization and recombination processes. We developed a model that satisfies this requirement. A similar model was used, e.g., in Ref. 4, to calculate the ion content of a plasma and its radiation properties. In our atomic model we describe in detail the ground states of ions with all the ionization states that we wish to include in the mathematical model. This allows us to correctly describe the dynamics of the ion content, both in the limit of very low plasma densities (i.e., in the so-called corona limit) and in the limit of local thermodynamic equilibrium, where the ion content is determined by the Saha equations. However, since the process of "quenching" of the ion content is quite time-dependent, it is necessary to compute correctly the influence of excited states on the rates of ionization (so-called multistep ionization) and recombination (three-particle recombination). Therefore, in our model we assumed that each ion has several excited states with principal quantum number n greater than n_0, the principal quantum number of the ground state. The fine structure of the levels is not included. For all levels of an individual ion except the ground state, the ionization energy I is calculated from the expression for a "hydrogen-like" ion, where

$$I=\frac{Z^2\mathrm{Ry}}{n^2};$$

here $Z=z+1$ is the spectroscopic symbol for the ion and Ry=13.6 eV is the ionization potential of a hydrogen atom. For the ground states the ionization energies are calculated using screening constants.[5] The radiative probabilities are calculated using oscillator strengths for the hydrogen atom, the rate of excitation by thermal electrons using the semiempirical formula of Van Regemorter.[6] The ionization rates for the ground states are computed based on the semiempirical formula of Lotz.[7] Ionization rates for excited levels are determined from the classical Thompson formula.[8] The photorecombination rates were obtained from the photoionization cross section for hydrogenic ions. The rates for three-particle recombination are calculated from the rates of ionization by thermal electrons using the detailed-balance relation. For two-electron recombination we used the semiempirical Burgess approach.[9] Photo- and three-particle recombination processes were included in the kinetic model for transitions from the ground state of an ion to all excited levels of a daughter ion of lower ionization state, while the corresponding ionization processes were included for transitions from all excited states of an ion to the ground level of a daughter at the next stage of ionization. Two-electron re-

combination was included only for ground states. This model gives a satisfactory description of the kinetics of hydrogenic ions if it is not necessary to include the fine structure of the levels. For other ions this approach makes it possible to include the influence of excited levels on the ion content of the plasma. In our model we were able to vary both the number of ionization states included and the number of "hydrogenic" levels over a wide range. The relative populations are found by solving the system of kinetic equations

$$\frac{d\mathbf{c}(r,t)}{dt}=K\mathbf{c}(r,t).$$

The vector $\mathbf{c}(r,t)$ denotes the set of relative populations of all the included states at time t at a point with coordinates r: $\mathbf{c}=\{c_1,\ldots,c_L\}$, $c_l=n_l/n_{\text{tot}}$, where n_l is the population of level l and n_{tot} is the total density of all the ions, i.e., $n_{\text{tot}}=\Sigma_{l=1}^{L}n_l$. The matrix K describes all possible elementary processes that lead to transitions between the different states.

The atomic model included stages of ionization of Pb from neutral atoms to Pb^{+40}. Each ion had up to four excited hydrogenic levels, so that the total number of states participating in the model exceeded 220. The tests we carried out showed that increasing the number of hydrogenic levels in the atomic model to 10 for each of the lead ions made only an insignificant change in the charge state of the plasma (a few percent in the value $\langle z\rangle$ over the region that gives the largest contribution to the collector signal).

The equations of the atomic model were solved self-consistently with the equations of gas dynamics. Energy losses to ionization and to excitation and heating of the plasma during recombination were included in the energy balance equation.

6. RESULTS OF CALCULATIONS

Our one-dimensional calculations were carried out in spherical geometry. Note that the initial target radius R_0 was a free parameter in our one-dimensional geometry, which we determined from the condition that the computed and experimental data coincide.

The length of the laser pulse, whose profile was a Gaussian, was taken to equal 20 ns with a maximum laser power flux density $P_0=3\cdot10^{13}$ W/cm^2. This value of P_0 corresponds to the maximum value of power flux density, taken at the initial radius of the target. During the pulse the critical surface moves out to a larger radius and the value of the power flux density at the surface becomes much smaller than in the absence of plasma expansion.

In Fig. 5 we show the time dependence of the collector current density and partial contributions from various ionization states (for $R_0=100$ μm), obtained from the one-dimensional model. These dependences, in keeping with the experimental scheme for the TIR-1 apparatus, were determined at a distance of 300 cm from the center of the target. It is clear from Fig. 5 that the primary output contribution to the collector signal comes from five or six ionization states. On this figure we show the time dependence of the average plasma ion charge $\langle z\rangle$. It turns out that the value of $\langle z\rangle$ corresponding to the maximum collector current is almost

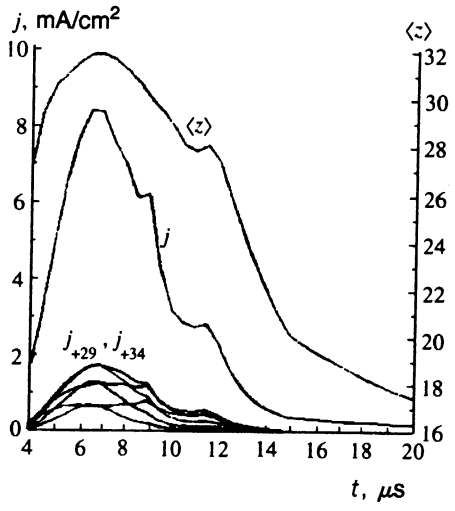

FIG. 5. Computed time dependence of the total current density of lead ions j and average ion plasma charge $\langle z\rangle$, obtained in a one-dimensional model ($j_{+29},\ldots,j_{+34}$ are partial currents for the ions $Pb^{+29},\ldots,Pb^{+34}$).

always equal to the charge of the ion that gives the largest contribution to the maximum value of collector current. The maximum value of $\langle z\rangle$ occurs at later times than the maximum of the collector signal. There is rather good agreement between the experimental data for $\langle z\rangle$ and the data obtained from one-dimensional calculations. However, the computed values of the maximum collector current density greatly exceed the experimental values. Thus, using the TIR-1 apparatus with $P_0\approx3\cdot10^{13}$ W/cm^2 we obtain a value of the maximum collector current density $j_{\max}=1.5$ mA/cm^2; the one-dimensional calculation gives $j_{\max}=8.5$ mA/cm^2. Our series of one-dimensional calculations for a fixed laser power density $P_0=3\cdot10^{13}$ W/cm^2 and values of the initial target radius $R_0=50$, 100, 200 μm give values of $\langle z\rangle=24.2$, 31.8, 34.4 respectively, and $j_{\max}=1.9$, 8.4, 25 mA/cm^2. This strong dependence of the results on R_0 is a serious defect of the one-dimensional model, which severely limits its usefulness in interpreting the experimental data.

In this work, our experiments were directed towards obtaining the maximum possible ionization states of lead. It is obvious that as the power density of the laser radiation increases for a fixed pulse duration, the average level of ionization $\langle z\rangle$ also increases.

In order to compute the dependence of the ion beam parameters on the pulse length, we carried out a series of one-dimensional calculations. The total Gaussian pulse length $2\sigma_t$ was taken to be 4, 20, and 100 ns for a fixed value of $P_0=3\cdot10^{13}$ W/cm^2. The results are shown in Table I. In this calculation, the primary contribution to the collector cur-

TABLE I. Maximum collector current density and the average ion charge at the time of this maximum, calculated in the one-dimensional model, versus the length of the laser pulse.

$2\sigma_t$, ns	4	20	100
j, mA·cm^{-2}	0.31/0.28	8.53	290
$\langle z\rangle$	26.4/16.5	31.9	34.0

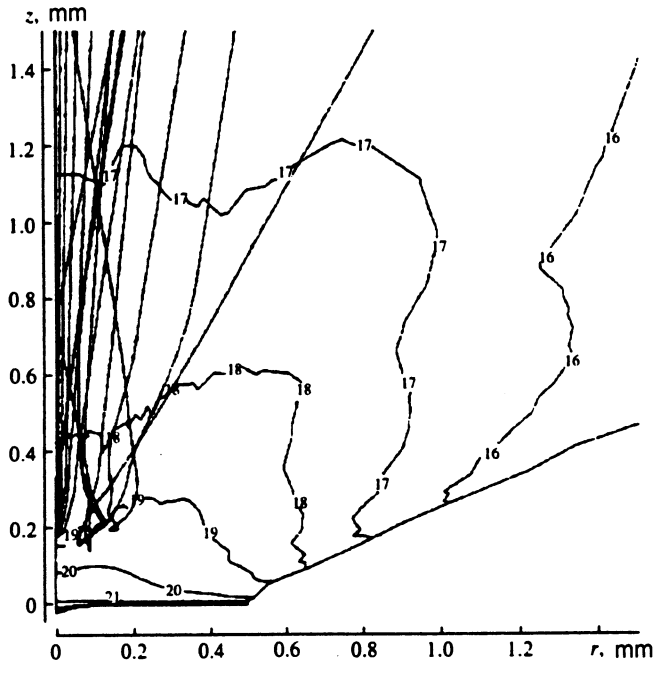

FIG. 6. Contours of constant electron density labeled by values of $\log n_e$, and laser ray trajectories in a square region with side 1500 μm at the instant when the laser pulse is a maximum (15 ns).

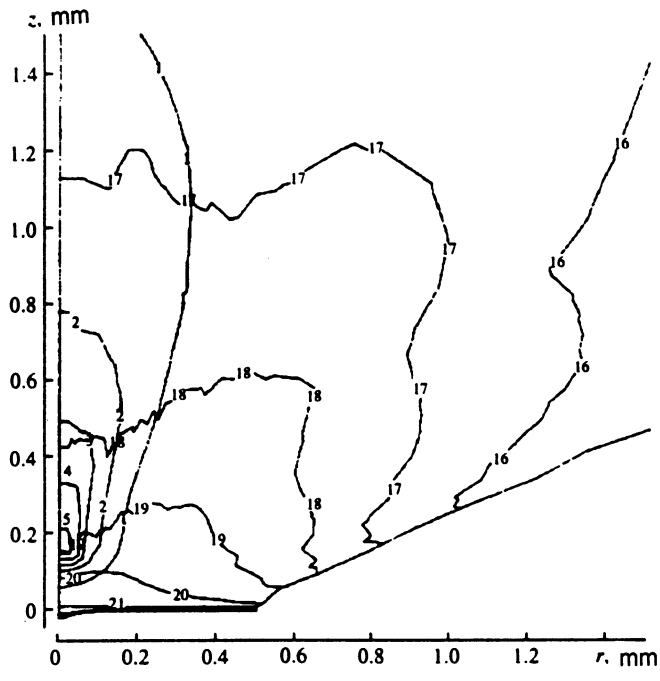

FIG. 7. Electron density contours labeled by values of $\log n_e$ and electron temperature contours. The numbers 5, 4, 3, 2, 1 correspond to values 0.9, 0.7, 0.5, 0.3, 0.1 of the maximum electron temperature T_e=1800 eV at time t=15 ns.

rent for the shortest (4 ns) pulse comes from two groups of ions: a high-charge group with $\langle z\rangle$=22–30 and a low-charge group with $\langle z\rangle$=13–19. The second group determines the total current 8 μs after the first group. If we further decrease the laser pulse length, only the maximum of the collector current connected with the second low-charge group remains. For long pulse lengths, the high-charge group dominates. Therefore, for fixed values of P_0, the way to obtain the maximum possible degree of ionization is to use rather long pulses with τ>10 ns.

In the two-dimensional model the total number of computational cells is orders of magnitude larger than in the one-dimensional model. For two dimensions the computation time increases even faster, which hinders systematic calculations that use the full kinetic model. Therefore, we developed a model for the two-dimensional case in which the quantities $\langle z\rangle$, $\langle z^2\rangle$ and the energy expended in ionization and excitation were determined at each time step based on tables computed previously under the assumption that the ion content is stationary.

At the initial time we specify the position of Lagrangian particles in the two-dimensional model, i.e., markers that move together with the material. At these markers we record the temperature and density dynamics, and at the end of the two-dimensional calculations we compute the population kinetics at each marker using the time-dependent model. Calculations based on this procedure are in good agreement with calculations based on the full model both for the distribution of charge at the markers and for the collector current.

In these calculations the CO_2 laser pulse was simulated by a Gaussian distribution of power flux at the focusing spot and a Gaussian temporal profile:

$$P=P_0\exp\left(-\frac{(t-t_0)^2}{\sigma_t^2}\right)\exp\left(-\frac{r^2}{\sigma_r^2}\right).$$

Our baseline pulse ($P_0=3\cdot10^{13}$ W/cm^2, σ_t=12.5 ns, σ_r=35 μm, radius of the illuminated portion of the surface 100 μm) corresponded to the illumination geometry for experiments using the TIR-1 apparatus. The laser beam was directed along the z axis in a cylindrical (r,z) geometry. The calculations were carried out on a grid of 20×50 cells in the r and z directions. At the initial time the target was a rectangle with dimensions 500×5 μm^2.

Ablation of material was rapid at the center of the focal spot, and the critical density surface moved out from the target to a distance of about 250 μm in the course of the first 1.5–2 ns after the start of the two-dimensional calculation. Initially, this surface is convex and a portion of the beam is scattered. Then an indentation in the density profile forms on the axis, with a diameter approximately equal to the beam diameter. This makes additional subfocusing of the beam possible (within the framework of the geometric-optics model used here), which leads to a small increase in the absorption and higher electron temperatures—up to 1.5–2 keV (in contrast to 1 keV in the one-dimensional model).

Figures 6–8 show half the axial cross section of the plasma spot in the cylindrical geometry. Figure 6 shows contours of constant electron density and laser ray trajectories in a region of size 1500×1500 μm^2 at time 15 ns (the maximum of the laser pulse). Figure 7 shows contours of electron temperature T_e and electron density n_e. In contrast to the predictions of calculations in spherical geometry, in two di-

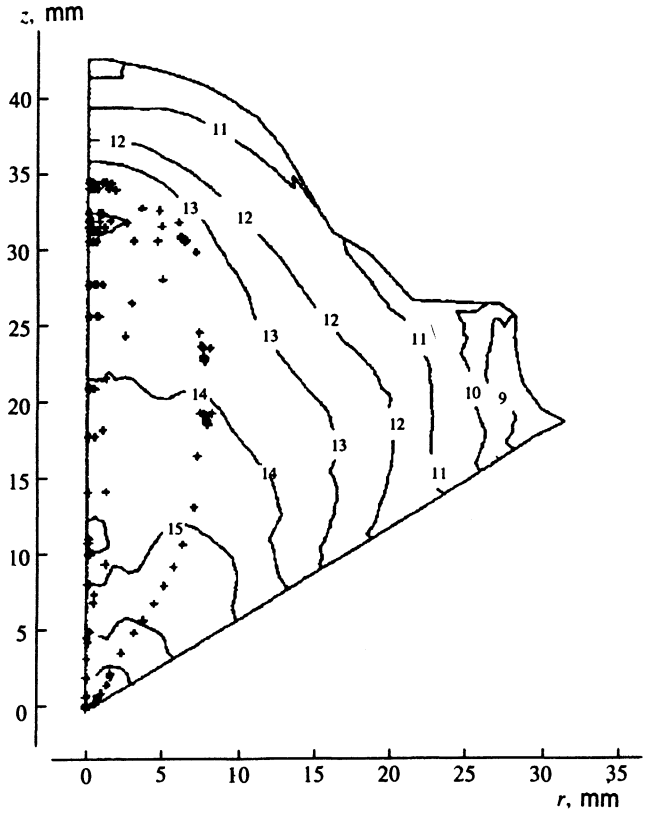

FIG. 8. Configuration of the computation region at time 100 ns and electron density contours labeled by values of log n_e. The crosses show the positions of the markers.

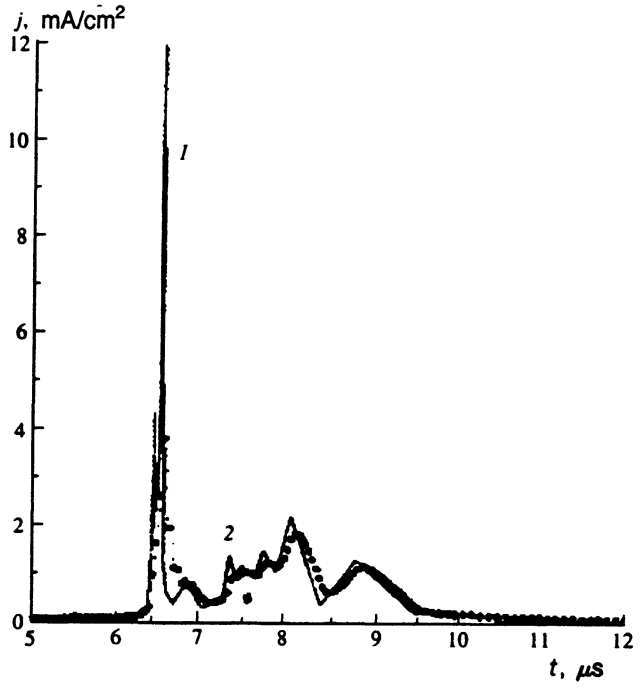

FIG. 9. Computed time dependence of the collector current density obtained in the two-dimensional model (*1*), and the same dependence including the effect of the equivalent electric circuit of the measurement setup (*2*).

mensions the electron thermal conductivity is not effective enough to equilibrate the temperature throughout the corona.

Figure 8 show the configuration of the computation region at time 100 ns. In this figure isolines of the electron density and the positions of the markers are shown. At the initial time, some of the markers were located in a rectangular region with dimensions 20×1 μm^2, while the rest, which describe the shape of the plasma spot, were located horizontally (z=const).

Figure 9 shows the time dependence of the collector current density determined from the results of the two-dimensional calculation at a distance 300 cm from the target surface (curve *1*). The sharp peak in the collector current is associated with a density increase (a compression wave) in the plasma that takes place at the trailing edge of the laser pulse as a result of nonuniformity in the absorption of the laser radiation. This rise in density appeared in all our calculations as the parameters of motion of the model were varied, i.e., the coefficient of boundedness of the electron thermal conductivity, the absorption model, and the atomic model. When we compare the calculated collector signal with the experimental signal, we have to keep in mind the following facts. First of all, the experimental curve shown in Fig. 4a was also modulated. In other shots in this series of experiments, we observed modulations of the collector signal that could reach 100% for a two- to three-peak signal structure. At lower laser radiation power densities (Fig. 4b), both the collector current and the ion spectra had a multipeaked structure. Secondly, the temporal resolution with which the collector signal shown in Fig. 4a was measured was too low to reveal peaks of width ~10 ns, of the sort that appear in the calculated curves. In Fig. 9 (curve *2*) we show the collector current density computed with the inclusion of transient processes in the equivalent electric circuit of the measurement setup. It is obvious that the agreement between the calculated and experimental curves is considerably improved in this case (Fig. 4a). Thirdly, as we mentioned in Sec. 4, the calculations do not include processes that accompany the extraction of the ion beam from the laser plasma. In particular, the presence of several grids with overall transmission of 40% in the real scheme for extraction-measurement of the ion current can distort the temporal fine structure of the latter.

7. CONCLUSION

We have investigated experimentally the ion content of a plasma formed by a powerful CO_2 laser beam at the surface of a target made of Pb.

We have developed a computational model to describe a laser plasma with a high ionization multiplicity.

The results of calculations based on the one-dimensional model agree qualitatively with experiment; however, the presence of a free parameter (the initial radius of the spherical target) considerably reduces the reliability of the numerical data. The two-dimensional model gives results in good agreement with the experimental data.

Our experiments and calculations show that, at a power density of $3\cdot10^{13}$ W/cm^2 of the CO_2 laser, the largest contri-

bution to the collector current comes from lead ions with maximum ionization multiplicities 28–32. This group of high-charge-state ions is well-separated both from the lead ions with lower multiplicity and from low-charge impurities.

In order to achieve a high ionization state, we found it more efficient to use rather long laser pulses of ~10 ns or more for the CO_2 laser radiation ($\lambda=10$ μm, $n_e^{cr}=10^{19}$ cm^{-3}).

The collector signal (and also the ion spectrum) had a peaked structure in both the experiments and in calculations based on the two-dimensional model. The magnitude of the modulation was very large, sometimes as high as 100%. A possible reason for the appearance of this type of oscillation is the generation of a compression wave (due to nonuniformity in the absorption of the laser radiation), which propagates in the direction of decreasing plasma density.

[1] A. E. Akimov, V. Yu. Baranov, V. L. Borzenko *et al.* Preprint IAE No. 3559, IAE, Moscow (1992).
[2] S. M. Kozochkin, K. N. Makarov, Yu. A. Satov *et al.* Preprint IAE No. 5635/7, IAE, Moscow (1993).
[3] D. C. Eder, Phys. Fluids B1 **12**, 2462 (1989).
[4] *Laser Program Annual Report*, LLNL, Livermore (1987), pp. 2–81.
[5] R. M. More, J. Quant. Spectrosc. Radiative Transfer **27**, 345 (1982).
[6] H. Van Regemorter, Astrophys. J. **132**, 906 (1962).
[7] W. Lotz, Zs. Physik **232**, 101 (1970).
[8] D. L. Book, *NRL Plasma Formulary*, NRL, Washington (1987).
[9] A. Burgess, Astrophys. J. **139**, 776 (1964).

Translated byFrank J. Crowne